

Least invasive in vivo imaging using harmonic generation microscopy

Szu-Yu Chen^a, Shih-Peng Tai^a, Cho-Shuen Hsieh^a, Chao-Yu Chen^f, Che-Hang Yu^a, Yen-Wei Lee^a,
Wen-Jeng Lee^c, Shee-Uan Chen^e, Fu-Hsiung Chang^f and Chi-Kuang Sun^{*a,b}

^aGraduate Institute of Photonics and Optoelectronics and Department of Electrical Engineering,
National Taiwan University, Taipei 10617 Taiwan, R.O.C.

^bResearch Center for Applied Sciences, Academia Sinica, Taipei 10617 Taiwan, R.O.C.

^cGraduate Institute of Electrical Engineering, National Taiwan University, Taipei 10617 Taiwan,
R.O.C.

^dGraduate Institute of clinical Medicine, National Taiwan University, No.1, Sec.4, Roosevelt Road,
Taipei, 10617 Taiwan, R.O.C.

^eDepartment of Obstetrics and Gynecology, College of Medicine, National Taiwan University, No.1,
Sec.4, Roosevelt Road, Taipei, 10617 Taiwan, R.O.C.

^fInstitute of Biochemistry and Molecular Biology, College of Medicine, National Taiwan University,
No.1, Sec.4, Roosevelt Road, Taipei, 10617 Taiwan, R.O.C.

ABSTRACT

In this manuscript, we review the physics and recent developments of the least invasive optical higher harmonic generation microscopy, with an emphasis on the in vivo molecular imaging applications. Optical higher harmonic-generations, including second harmonic generation (SHG) and third harmonic generation (THG), leave no energy deposition to the interacted matters due to their energy-conservation characteristic, providing the “noninvasiveness” nature desirable for clinical studies. Combined with their nonlinearity, harmonic generation microscopy provides three-dimensional sectioning capability, offering new insights into live samples. By choosing the lasers working in the high penetration window, we have recently developed a least-invasive *in vivo* light microscopy with submicron 3D resolution and high penetration, utilizing endogenous and resonantly-enhanced multi-harmonic-generation signals in live specimens, with focused applications on the developmental biology study and clinical virtual biopsy.

Keywords: second harmonic generation, third harmonic generation, higher harmonic generation, harmonic generation microscopy, noninvasive microscopy, virtual biopsy, molecular imaging, resonance enhancement

1. INTRODUCTION

Higher harmonic generations, including second-harmonic-generation (SHG) and third-harmonic-generation (THG) processes, are known to leave no energy deposition to the interacted matters due to the virtual-transition characteristic¹. In contrast to the absorption-induced-fluorescence processes that require energy deposition and electron transitions, the higher harmonic generation processes provide the optical noninvasive nature desired for microscopy applications, especially for long-term observing the dynamic changes of live samples. Different from single-photon and multi-photon fluorescence, no energy release is required during the harmonic-generation process, thus no cell damages and no photobleaching are expected. With a nonlinear nature similar to the multi-photon excited fluorescence, the generated SHG intensity depends on the square of the incident light intensity, while the generated THG intensity depends on the third power of the incident light intensity¹. These dependencies allow localized excitations to enable intrinsic optical sectioning and a sub-micron three-dimensional resolution similar or better than the two-photon fluorescence microscopy can be achieved². With a coherent nature during the generation processes, THG can be utilized as a general-purpose microscopic technique for morphological studies^{3,4} while SHG is sensitive to the local molecule arrangement and is particularly useful for structural biomolecule studies^{3,5}. THG is known to be a fundamental physical process of which the THG intensity peaks when the foci of the strongly focused optical beams are located at the material interfaces⁶, including the interfaces inside a cell. From 1996, many applications were carried out to reveal the structures of the biological tissues by utilizing the interface sensitivity of the THG microscopy⁷⁻¹¹. On the other hand, SHG contrast in biological specimens can be provided by ordered arrangement of highly asymmetric bio-molecules, where the optical centro-

symmetry is broken, such as stacked membranes^{2,5} and aligned protein structures^{1,5,12}, including mitotic spindles^{4,13}, muscle fibers^{3,13}, and collagen fibrils¹. However, currently adopt GFP- or SHG-based techniques are strongly limited by the light source and thus the penetration depth and cell viability. In previous studies, with a 80 MHz Ti:sapphire laser and a NA~1 objective, less than 2-7 mW average power can be applied to live samples to prevent optical damages¹⁴. As the excitation laser wavelength is increased to 1047 nm, the maximum average illumination power can only be increased to 13 mW to provide suitable cell viability¹⁵.

To enable the long-term *in vivo* observation deep inside a thick embryo, stronger illumination power and deeper penetration depth is desired. Recently, it was shown that by using a laser at 1230 nm, deep penetration³ and high cell viability⁴ can be provided even with a strong illumination power of 100 mW. It is thus highly desired to apply the 1230 nm light for *in vivo* long-term observation of mammal embryo development. In this article, the least invasive imaging of mouse embryos will be presented. The 3D images of mouse embryos which are taken from harmonic generation microscopy can probably provide the helpful information in observing mammal embryos. The SHG signals arose from the spindle fibers provide us the information of the oocyte being mature or not. Combined with the polar body position shown by THG signals, the score of the embryos can be decided. The SHG signal intensity of zona pellucida and the appearance of two pronuclei declare the fertilization of zygote. With its optical sectioning property, high penetration depth, and much-reduced photodamages, harmonic generation microscopy, the least invasive imaging method, provides superb imaging capability for dynamic developmental studies of vertebrate embryos in the future.

As mentioned above, since THG was utilized as a general-purpose microscopic technique for morphological studies in the past, THG microscopy was rarely used to perform molecular imaging. Here, we have also demonstrated the first *in vivo* molecular resonant enhanced epi-THG microscopy to image erythrocytes by matching THG wavelength with the Soret transition of oxyhemoglobin. Besides, we also developed several bright THG contrast agents including metal nanoparticles and lipid enclosed quantum dots. The studies with lipid enclosed quantum dots will be shown in this article. By conjugating THG contrast agents with anti-Her2 antibodies, Her-2 overexpression of live cancer cells has been successfully demonstrated by using epi-HGM for the first time. By injection of tumor cells with THG contrast agents labeling into the dermis tissue of nude mice, the tumor cells can be clearly and continuously imaged *in vivo* with epi-THG microscopy in the subcutaneous tissue over a week.

2. METHODOLOGY

2.1 System setup

Our home-built laser scanning harmonic generation microscopy (HGM) system is adapted from an Olympus FV300 scanning unit combined with an Olympus BX51 upright microscope while all optics are modified to allow the passage of the 1200~1350nm infrared light. A home-built Cr:forsterite laser, which operates at 1230nm with a repetition rate of 110MHz and a pulse width of 130fs (300-mW average output), is used as the light source to allow both SHG/THG to fall within the visible spectrum and also provide advantages of low illumination attenuation. Real-time 2D scanning is accomplished with a pair of high-speed galvanometer mirrors inside the FV300. The collimated laser beam is coupled into the scanning system connecting to the Olympus BX51 microscope with an aperture fitting tube lens. Through a 2-mm-working-distance high numerical-aperture (NA) infrared objective (LUMPlanF1/IR 60X/water/NA0.9, Olympus), the excitation laser pulse is focused into the desired location inside the specimen and scanning with a spot size close to its diffraction limit. In the observation of mammal embryo development, since the thickness of the embryo was about 100 μ m, which was thin enough for signals to pass through, a forward-collected geometry was used. The forward-propagating optical harmonics signals are collected by a high-NA (1.4) oil-immersion condenser and guided into two photomultiplier tubes (PMT), which are synchronized with the galvanometer mirrors and used to respectively record the interference-filtered SHG and THG signals point by point to form 2D sectioned images. On the other hand, in the studies of the THG contrast agents, since *in vivo* observation was performed on the animal models, a backward- collected geometry was used in this case. The backward-propagating harmonics signals are collected by the same objective and reflected by a dichroic mirror, which separated infrared laser beam and the harmonics signals guided into two photomultiplier tubes (PMT). Besides, stereographic 3D images of the skin can be obtained by controlling the depth of focus inside the specimens, and be used to analyze the thickening of skin. In this article, the harmonics signals collected are represented by two different pseudocolors, green for SHG and red for THG.

2.2 Embryo collection and preparation

In the research of mammal embryo development, the female mice of outbred ICR strain aged 6 to 8 weeks were induced to superovulate by intraperitoneal injection of 10 IU of pregnant mare serum gonadotropin (Sigma, St. Louis, MO). Forty-eight hours after the injections, they were injected with 10 IU of hCG (Organon, Oss, The Netherlands) to trigger ovulation. Each female mouse was placed with a male for mating. Eighteen hours after mating, the mating was confirmed by the presence of a vaginal plug. Oocyte, 2 cells, and 4 cells were collected from the oviduct and were cultured with human tubal fluid plus 4 mg/mL of human serum albumin (HAS; Sigma) in an atmosphere of 5% CO₂ in air at 37°C¹⁶. After ovulation, the ovary released an oocyte, which enters the oviduct. Entry of a sperm caused the oocyte to complete meiosis and became an ovum. Fertilization occurred when the nuclei of the ovum and sperm fused, producing a zygote. Cleavage began in the oviduct as the embryo was moved toward the uterus, 2 cells, 4 cells, 8 cells, and so on. The blastocyst implanted in the endometrium about 4.5 days after conception.

3. THG CONTRAST AGENTS

In our HGM, we combine SHG and THG to section biological specimens while THG can provide morphologic information including the size, shape, and distribution of cells with a sub-micron spatial resolution. However, THG is generally regarded as a morphological imaging tool due to its interface-sensitive nature, with limited capability for molecular imaging. Therefore, it should be highly desirable to develop THG contrast agents to trace the functions of a specific molecule, taking advantage of the noninvasive nature of the THG process. Besides, a bright THG contrast agent can also increase the penetration depth of epi-THG microscopy. Through molecular-resonant third-harmonic-generation in hemoglobin, we have demonstrated *in vivo* molecular resonant enhanced THG microscopy of erythrocytes without using fluorescence. At the same time, we have also developed several exogenous THG contrast agents such as lipid enclosed quantum dots for least invasive molecular imaging without energy deposition.

3.1 Endogenous THG contrast agents – Hemoglobin

To develop THG molecular imaging, THG at target should be stronger than the background, which means we need a mechanism for enhancing THG at a specific cellular site. The straight way is matching THG or fundamental frequency with a real transition frequency of a specific endogenous biomolecule. Through molecular-resonant third-harmonic-generation in hemoglobin, we have demonstrated the *in vivo* molecular resonant enhanced THG microscopy of erythrocytes without using fluorescence. Recently, hemoglobin has attracted lots of scientific interests, since hemoglobin is one of important clinical indexes and is the main content of erythrocytes. Besides, hemoglobin is a non fluorescent chromophore¹⁷, and thus hard to be observed with fluorescence microscopy. The hemoglobin in the erythrocytes is usually in the oxygenated form and with the strong Soret transition at ~410nm¹⁷ which is visible. It is therefore expected that this Soret transition of oxyhemoglobin should resonance enhance the 1230 nm excited THG signals. Schaller *et al.* in the previous work demonstrated a near-field THG scanning imaging study of a dried red blood cell by qualitative showing that their image contrast was best when their THG wavelength tuned near the Soret transition in oxyhemoglobin. However, that work did not provide information at the resonance peak wavelength of hemoglobin and motivates us to do a systematic and quantitative study of oxyhemoglobin.

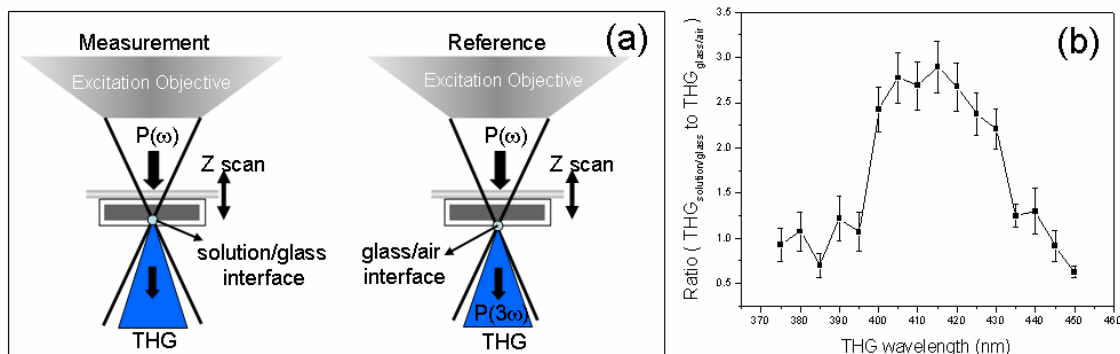


Fig. 1 Third-harmonic spectroscopic measurement procedure applied to the oxyhemoglobin solution. (a) Schematic showing the sample and the apparatus. Third-harmonic generated signal was collected from both the solution/glass interface and

the glass/air interface, and their intensity ratio was used to infer sample spectral properties. (b) Measured THG intensity ratio (THG at solution/glass interface to THG at glass/air interface) after normalization versus THG wavelength.

To measure the spectral response of THG in oxyhemoglobin, we followed the similar method used in a previous report¹⁸. We used the human hemoglobin (Sigma-Aldrich, H7379) for study. The hemoglobin solution with concentrations of 0.6 mM (~5g/dL) was contained in the microcuvette. The excitation source we used for this study is an optical parametric oscillator (OPO) pumped by a femtosecond Ti:sapphire laser (Coherent Inc, Mirra). The OPO is tunable from 1100nm-1600nm with 200fs pulse duration and the average output power 60mW-100mW, which is dependent on wavelength. We scanned through the solution-filled microcuvette along the propagation axis of the incident beam and collected third-harmonic signals from both the solution/glass and the glass/air interfaces (Fig. 1(a)). The third-harmonic power, $P(3\omega)$, traces out two bell-shaped profiles as the focus swept across the two interfaces. The peak of the profile centered on the lower solution/glass interface corresponds to $P(3\omega)_{\text{solution/glass}}$, and the peak of the profile centered on the bottom of the glass side corresponds to $P(3\omega)_{\text{glass/air}}$ and was used as the reference. The relation between THG intensity ratio and THG wavelength is shown in Fig. 1(b). Strong THG can be observed when excitation wavelength was tuned close to 3 times the wavelength of Soret transition. The resonant THG of hemoglobin can be observed from 400nm to 430nm (peak at 415nm) corresponding to the fundamental excitation wavelength of 1200nm-1290nm. About three times THG enhancement can be observed (Figure 1(b)), when the THG wavelength was tuned near the Soret transition of oxyhemoglobin.

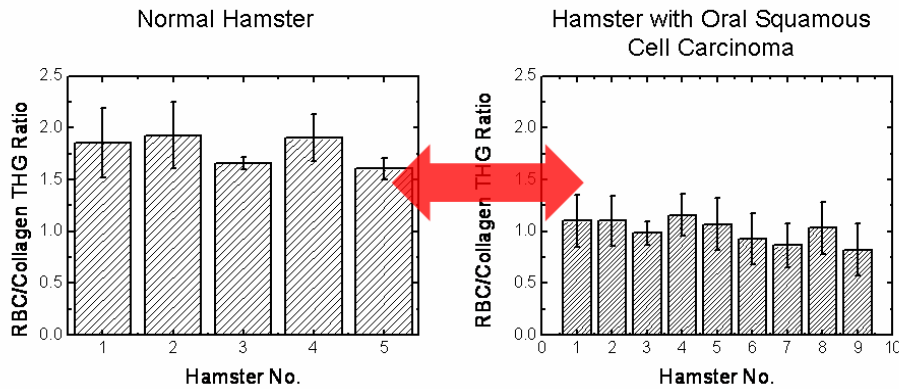


Fig. 2 The intensity ratio of THG_{RBC} to $\text{THG}_{\text{dermis}}$ measured from the oral cavity of 5 normal hamsters and 9 hamsters with oral squamous cell carcinoma. The average ratio obtained from the normal hamsters was about 1.7 and almost no enhancement (ratio~1) was found in the region with oral squamous cell carcinoma.

In the experiment described above, the hemoglobin oxygen saturation S_{HB} of the oxyhemoglobin was about 100%, and the THG enhancement was around 2.5 times at THG wavelength of 410nm. Based on this enhancement, in live tissues, it is quite easy to distinguish the erythrocytes from surround tissues. To verify this capability, the in vivo observation was carried out in the oral cavity of the hamster, including normal hamster and hamster with oral squamous cell carcinoma. After finding the erythrocytes, also called red blood cell (RBC), within the dermis, the THG intensity of both RBC and the surrounding dermis tissue (composed mostly with collagenous tissues and cells) was measured and averaged over 5 to 7 different areas, and then the ratio of THG_{RBC} to $\text{THG}_{\text{dermis}}$ could be obtained (Fig. 2). To perform the statistic analysis, the ratio was measured in 5 normal hamsters and 9 hamsters with oral squamous cell carcinoma. Comparing the ratio obtained in the normal hamster and hamster with oral squamous cell carcinoma, it was surprising to find that the level of THG enhancement in the two cases was different. The THG intensity was about 1.7 times enhanced in the RBCs in normal hamster oral mucosa but almost no enhancement was found in the RBCs in the cancerous tissue (Fig. 2). Moreover, both results were different from that measured from oxyhemoglobin (2.5 times enhancement) with S_{HB} of 100%. Compared with our spectroscopic measurement where 2.5 times enhancement corresponding to 100% oxygen level, our in vivo study with 1.7 times enhancement corresponds to ~47% oxygen level while no enhancement (1 time) indicates ~0% oxygen content, agreeing with previous studies. In the previous studies, the S_{HB} in the normal epithelium tissue like skin (human skin) was measured about 48.2%¹⁹, and S_{HB} usually became much lower around the cancerous tissues. Our study indicates that THG could provide an accurate way to non-invasively measure and analyze the S_{NB} in a

single RBC, and could be very useful for diagnosing some life-threatening diseases, in which changes of S_{HB} are involved.

3.2 Exogenous THG contrast agents – Lipid enclosed quantum dots

For molecules without absorption transition in the visible spectrum, the above mentioned resonance measurement will be hard to apply for in vivo imaging, due to strong UV absorption in tissue. Some exogenous contrast agent would be required. In the previous studies, metal nanoparticles have been used as THG contrast agents. However, sometimes the multi-photon excited fluorescence (MPEF) of metal nanoparticles covers a broad spectral band and will induce the crosstalk with THG signals²⁰. Therefore, it is highly desired to develop bright THG contrast agents in all excitation wavelengths with low and narrow band fluorescence. Here we show that lipid enclosed quantum dot can serve this purpose. The advantages of using lipid enclosed quantum dots include high THG efficiency and insensitive to excitation wavelength²¹. Besides, the crosstalk between MPEF and THG can be avoided due to narrow emission spectrum of MPEF from quantum dots and weak multi-photon fluorescence when excitation photon energy is smaller than half bandgap of quantum dots. In our study, the quantum dots we used as THG contrast agents are composed of CdSe and then enclosed by lipid layers to make a suspension in deionized water. Such lipid enclosed CdSe quantum dots were prepared by C.-Y. Chen from Prof. F.-H. Chang's group in National Taiwan University. The diameters of such lipid enclosed quantum dots can be controlled to be 30nm~200nm and their emission wavelength was ~580nm which was far from our THG wavelength (410nm). Besides, the lipid enclosure can reduce the toxicity of quantum dots. From Figure 3, efficient THG can be observed from lipid enclosed CdSe quantum dots (Fig. 3(h), (i)), as reported in previous studies about THG from lipid bodies²² and quantum dots²³.

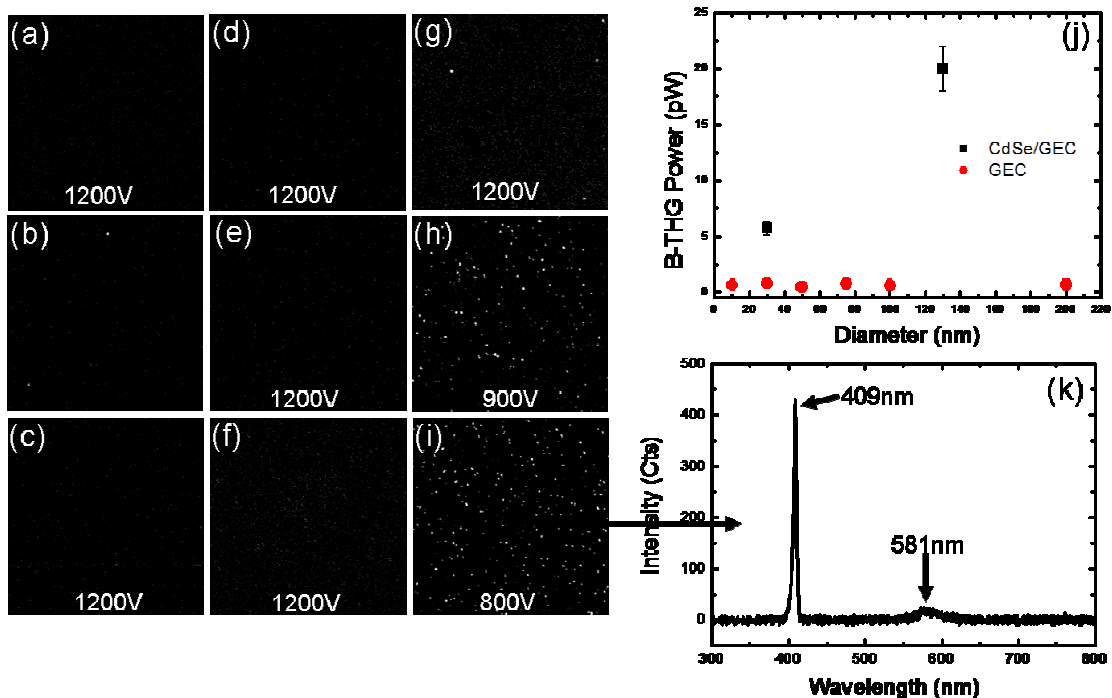


Fig. 3 The B-THG images of nano-materials in solutions. (a) deionized water; PMT Voltage: 1200V (b) GEC spheres 10nm in diameter; PMT Voltage: 1200V (c) GEC spheres 50nm in diameter; PMT Voltage: 1200V (d) GEC spheres 100nm in diameter; PMT Voltage: 1200V (e) GEC spheres 200nm in diameter; PMT Voltage: 1200V (f) DPPC spheres 100nm in diameter; PMT Voltage: 1200V (g) CdSe quantum dots 5nm in diameter; PMT Voltage: 1200V (h) CdSe/GEC spheres 30nm in diameter; PMT Voltage: 900V (i) CdSe/GEC spheres 130nm in diameter; PMT Voltage: 800V. Scale bar: 20 μ m (j) B-THG power vs. size of CdSe/CEC (square) and GEC (circle) nano-spheres. (k) Measured emission spectrum of the CdSe/GEC quantum dots excited by the fs Cr:fosterite laser.

To identify the origin of the strong THG we observed, we used our PMT based epi-HGM to measure B-THG intensities of different nano-materials in solution including CdSe quantum dots, lipid spheres, and lipid enclosed CdSe quantum dots (CdSe/lipid). Two kinds of lipid spheres made of 1, 2-dipalmitoyl-sn-glycero-3-phosphocholine (DPPC) and GEC (a novel lipid prepared by C.-Y. Chen from Prof. F.-H. Chang's group in National Taiwan University) were used in our measurement (Fig 3). Since huge THG intensity differs between those nanomaterials, different voltages (800V-1200V) were applied to PMT in the measurement. Figure 3(a-j) shows the measured average THG power of single CdSe/GEC and GEC nano-spheres with different sizes after calibrating PMT with applied voltages. Our results show that we are barely able to detect the generated THG from lipid nano-spheres even with a 200nm diameter (Fig 3(e)). The observed THG from CdSe quantum dots (5nm in diameters, used to synthesize lipid enclosed quantum dots) was also very weak. On the other hand, compared with GEC nanospheres, 10X (30nm) -40X (130nm) stronger THG of CdSe/GEC nanospheres can be observed (Fig. 3(j)). Therefore, the observed strong THG should come from neither lipid spheres nor just small CdSe quantum dots (<10nm). Due to the fact that THG is highly sensitive to interfaces⁷ and the THG intensity nonlinearly increases with size when the particle is much smaller than the laser spot size²⁴, the observed strong THG should thus be contributed from combinations of multiple interfaces in one lipid nano-sphere with multiple quantum dot enclosure and size effect. Besides, we also measured the emission spectrum of the quantum dots excited by our fs Cr:fosterite laser (Fig. 3 (k)). We can observe no cross talk between THG and MPEF. It is shown that using our developed THG microscope to image such lipid enclosed CdSe quantum dots is a better way since THG intensity of lipid enclosed CdSe quantum dots is 5X~20X of MPEF when the quantum dots are excited with a femtosecond 1230nm light (Fig. 3 (k)).

To demonstrate that CdSe/GEC nano-spheres can be used as THG contrast agents in cells, we delivered CdSe/GEC nanospheres into HeLa cells and then imaged with the THG (Fig. 4(a)) and MPEF (Fig. 4(b)) microscopy. From the THG image of HeLa cells with CdSe/GEC labeling (Fig. 4(a)), rich THG bright spots can be observed in cells. The MPEF image provides the position information of the applied CdSe/GEC nanoparticles. By comparing THG and MPEF images, most MPEF spots overlap with those in the THG image (Fig. 4(c)) and thus we can confirm that CdSe/GEC nanoparticles are efficient THG generators.

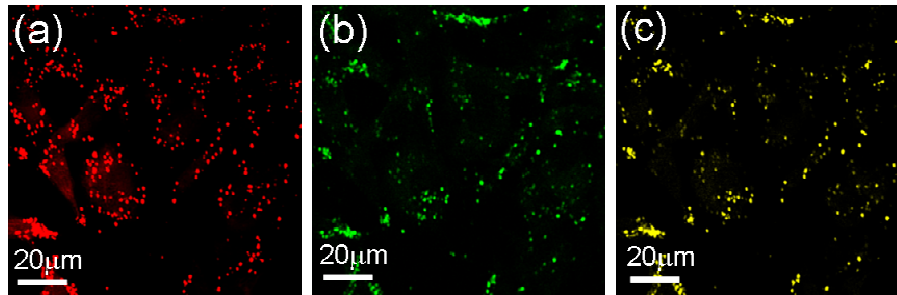


Fig. 4 Images of HeLa cells with CdSe/GEC labeling taken by (a) THG microscopy (b) MPEF microscopy. (c) The overlap of (a) and (b).

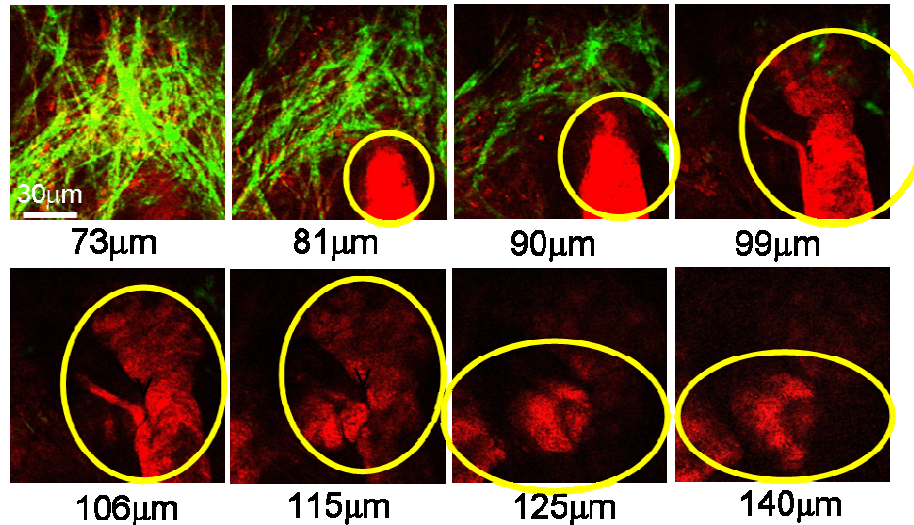


Fig. 5 Example of horizontal sections in the nude mouse skin of induced CT26 tumor region with CdSe/GEC labeling taken by epi-HGM microscopy *in vivo*. In the figure, the green color is used to represent B-SHG and red color to represent B-THG. Strong THG from tumor cells inside the yellow circle with CdSe/GEC labeling can be clearly observed in the subcutaneous tissue.

To demonstrate potential clinical applications in the future, we performed the preliminary study by inducing human colonic cancerous tumor in the skin of nude mice (Nar1: ICR-Foxn1nu) as the animal model. The human colonic cancer cells CT-26 from ATCC (MD, USA) were cultured in RPMI with 10% heat-inactivated fetal bovine serum supplementation. Cells were routinely maintained at 37°C with supplementation of 5% CO₂ and then the lipid enclosed quantum dots are added in the culture medium and cultured with CT26 cell lines over 24hrs. In this study, the lipid used to enclose CdSe quantum dots is GEC since the GEC nanospheres can easily penetrate into cells. For tumor induction, 5×10^5 CT26 cells with and without CdSe/GEC quantum dots labeling were injected into dermis tissue of the nude mouse. After one week, our epi-HGM was used to image the tumor region. In the experiment, the observed nude mouse was anaesthetized first, and then rested under our THG microscope including an electric blanket to maintain the body temperature.

In the control experiment, we have taken B-THG images of the induced colonic tumor without CdSe/GEC labeling in three nude mice (not shown in this article) with over five different tumor regions in each mouse. In most cases with the same PMT voltage as the experiment shown in Fig. 5, we can not observe significant THG from cells with a depth over 100µm under epidermis. On the other hand, THG from tumor cells with CdSe/GEC labeling can be observed even in depth over 100µm under epidermis (Fig. 5). Therefore, by using lipid enclosed CdSe quantum dots as contrast agents, distribution of cancer cells in the subcutaneous tissue can be observed and thus ideal for tracing tumor progression *in vivo* in the future.

4. MAMMAL EMBRYO DEVELOPMENT

Besides gene expression, embryogenesis is another important issue in embryology. Many couples have to face infertility nowadays. The reason includes tubal damage, failure of ovulation, and sperm defect. In the concept of eugenics, the selection of embryos has become a key project. In clinical practice, there are subjective protocols for deciding which embryos should be transferred to their mothers. The obstetrics and gynecology doctors do not dare to use laser scanning microscopy to select IVF or ICSI oocytes and zygotes. Its challenge is to maintain embryo viability following prolonged exposure to excitation illumination¹¹. The optical technologies they use, such as Differential Interference Contrast Microscopy (DIC) or optical microscope, cannot reveal spindle fibers. Polar scope, which can observe the specimens that are visible primarily due to their optically anisotropic character, reveals the spindle fibers in the oocyte²⁵, but do not have a high penetration depth, and therefore are unable to provide 3D reconstruction of the cell distribution and the detail inner structure of the embryo. HGM has previously provided the least invasive images deep inside the live zebrafish embryos²⁶ with high cell viability and should thus be an ideal tool for the least invasive cellular imaging in mammalian embryos. The structure of the inner cell mass (ICM) of the blastocyst, in particular, provides a good indication of

prospective embryo viability after transferring back to the mother. Due to the minimized photodamage and photobleaching effects, HGM is potentially ideal to assess the regularity of lineage for both the mouse and human. Much of the information about human embryonic development comes from studies of embryogenesis in the mouse. ICR mouse is the specimen of mammalian development and most techniques that are in current use with these stages of humans and farm animals are first devised in this species. In this part of manuscript, we demonstrate a 3D and *in vitro* HGM study of live ICR mouse embryo development dynamics with a sub-cellular spatial resolution.

4.1 Three-dimension images of mouse oocyte

Due to the localized excitation property of the nonlinear processes and the high penetration capability of the incident light, optical harmonic generation microscopy allows the least invasive observation of the whole mouse embryo development with a sub-micron 3D spatial resolution. The excellent depth-resolution and high-penetration capability of the optical harmonic generation microscopy are demonstrated in Figure 6. The 3D mouse oocyte structure can be completely resolved from the top surface of the oocyte to the bottom.

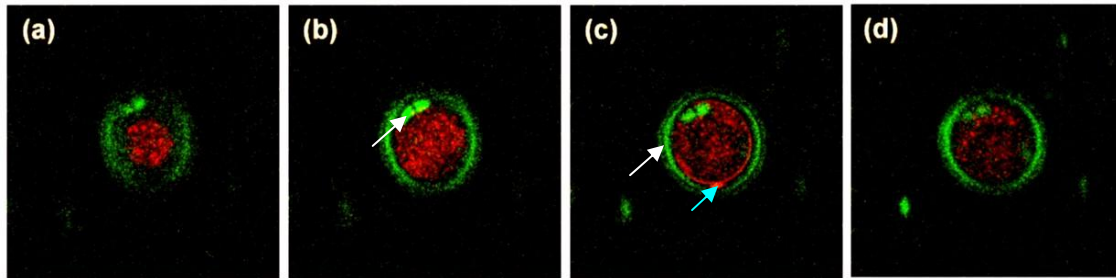


Fig. 6 Depth-resolved section series with combined SHG and THG signals inside the live mouse oocyte. (A) - (d) are at imaging depths from 10 μ m to 55 μ m relative to the embryo surface with a step of 15 μ m. Image size: 240 μ m \times 240 μ m.

4.2 In vitro observation of mouse embryos

For HGM observation of mouse embryo, the embryos were placed in a Petri dish filled with culture medium. The dish was put into a CO₂ incubator, MIU-IBC-I (Olympus) filled with 5% CO₂ and the medium was kept at about 37°C. Prior to fertilization in mice, the egg enlarged, divided by meiosis, and matured in its ovarian follicle until it reached a stage of meiotic division called metaphase II and released its first polar body (indicates by a blue arrow in Fig. 6(c)). The matured oocyte, a haploid cell that contained half the normal number of chromosomes, which was arrested at metaphase of meiosis and kept the spindle (indicates by a white arrow in Fig. 6(b)), was surrounded by a protective coat of noncellular material (made of extracellular matrix and glycoproteins), called the zona pellucida (indicated by a white arrow in Fig. 6(c)). Under HGM the zona pellucida contains 2 layers of SHG signals, a strong one and a weak one, with a dark layer between them. Compare to the polar scope images²⁷, the zona pellucida can be divided into 3 layers: a greyish-appearing outer layer (OL) with weaker SHG signals, a dark-appearing middle layer (ML), and a highly birefringent inner layer (IL).

For fertilization to occur, a sperm cell must bind to and penetrate the zona pellucida and the cell membrane of the oocyte, enter the oocyte cytoplasm, and form two pronuclei, one from the sperm and one from the oocyte. Figure 7 shows the HGM images of a live mouse embryo at 2P stage with different imaging depths. By scanning from the surface of the embryo to the bottom, we can clearly observe the two nuclei (white and blue arrow in figure 7) through THG signals. On the other hand, we can clearly see that the intensity of SHG is weaker than the oocyte, due to the changes of structure in zona pellucida, which forbid of next sperm cell to enter.

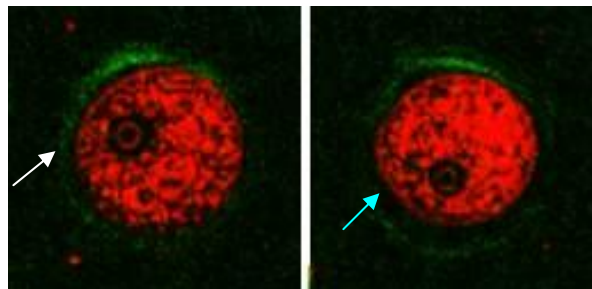


Fig. 7 HGM section images of the same 2P stage mouse embryo with different depth. The THG signals reveal the two nuclei (white and blue arrow). Image size: 120 μ m \times 120 μ m.

After fusion of the sperm and egg pronuclei, the cleavage began. During these initial cleavages, the resulting daughter cells did not enlarge in size. Rather, as the early cell division proceeded, the amount of cytoplasm of each daughter cell was reduced by half, and the total volume of the early embryo remained unchanged from that of the fertilized egg. After fertilization, the zygote was moved toward the uterus, a journey that took three to four days in mice. As it traveled, the zygote divided. The first cleavage produced two identical cells (Fig. 8(a)) and then divided again to produce four cells (Fig. 8(b)). If these cells separated, genetically identical embryos will be resulted, which is the basis of identical twinning. Usually, however, the cells remain together, dividing asynchronously to produce 8 cells, 16 cells, and so on. At about the eight-cell stage (Fig. 8(c)), the cell adhesion proteins were expressed and the embryo compacted, meaning that the formerly "loose" ball of cells, the blastomeres, huddled together in a tight array that were interconnected by gap junctions. By the 16-cell stage, the compacted embryo was termed a morula (Fig. 8(d)). In mice, the first evidence that cells had become specialized was when the outer cells of the 16-cell morula divided and produced an outer rim of cells—the trophectoderm—and an inner core of cells, the inner cell mass. Ultimately, the cells of the inner cell mass would give rise to all the tissues of the embryo's body. The trophectoderm, in turn, would generate the trophoblast cells of the chorion, the embryo's contribution to the extraembryonic tissue known as the placenta.

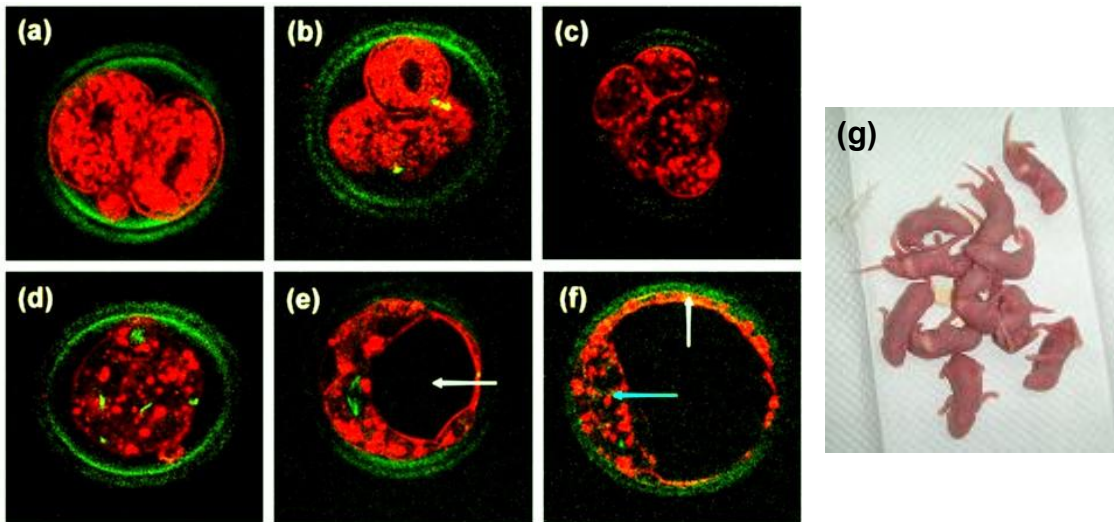


Fig. 8 HGM section images of ICR/mouse embryos at (a) two cells, (b) four cells, (c) eight cells, (d) morula (about 16 cells), and (e), (f) blastocyst stages. The difference of embryo size is because of different section depth of the embryos. (g) The observed embryos developed normally to healthy ICR mice. Image size: 120 μ m \times 120 μ m.

By embryonic day 3 (E3.0) in the development of ICR mouse, the embryo developed a cavity called the blastocoel (indicated by the arrow in Fig. 8(e)). It filled with a watery fluid secreted by trophectodermal cells and transported in from the exterior. As a result of cavitation and the physical separation and differentiation of the trophectoderm from the inner cell mass, the morula became a blastocyst (Fig. 8(f)). Its chief structural features are the outer sphere of flattened trophectoderm cells (which became the trophoblast (indicated by the white arrow in Fig. 8(f)), the small, round cells of the inner cell mass (Indicated by the blue arrow in Fig. 8(f)), and the fluid-filled blastocoel. These and other observations about the preimplantation blastocyst have led to recommendations about the importance of adapting the culture conditions to accommodate the changing nutritional requirements of the embryo when animal embryos were grown in the laboratory. At this stage of embryogenesis—about E4.0 in mice—that embryonic stem (ES) cells can be derived from the inner cell mass of the blastocyst.

In order to study if HGM is truly least invasive during mouse embryo observation, we have conducted a viability test. The embryos at 4 cell stage were taken from the mouse oviduct. Half of the live embryos were used as control set and were put in the MIU-IBC-I incubator for 10 mins without HGM observation, and then in the CO₂ incubator for 2.5 days. Another half of the embryos were put in the MIU-IBC-I incubator and scanned using HGM with 100mW laser power for 10 mins (total exposure = 20J per embryo), and then in the CO₂ incubator for 2.5 days. The surviving rate depends on those which develop to blastocyst. The viability of experimental set with HGM is 67% (6 embryos develops to blastocyst

out of 9), which is very close to the 70% of the control set (7 embryos develop to blastocyst out of 10). Moreover, most of the survived embryos have developed normally to healthy ICR mice (Fig. 8(g)), and this result confirmed the non-invasiveness of the HGM system.

5. CONCLUSION

To develop THG microscopy with molecular functionality, we proposed several endogenous and exogenous THG contrast agents. For the endogenous THG contrast agent, through matching THG wavelength with the Soret transition of oxyhemoglobin, we demonstrated *in vivo* molecular resonant enhanced epi-THG microscopy of erythrocytes imaging. We also showed that this molecular resonant enhanced epi-THG microscopy was ideal for capillary-related diagnosis and imaging embryo heart development. Moreover, the different THG intensity ratios we obtained may indicate the different S_{NB} in different tissues. It provides another way to non-invasively measure and analyze the S_{NB} , useful for diagnosing diseases, in which changes of S_{HB} are involved. For the exogenous THG contrast agent, through resonance and size effect to enhance THG, lipid enclosed CdSe nanospheres with ~100nm is shown to be a good candidate of THG contrast agents. By conjugating CdSe/DPPC nanospheres with anti-Her2 antibodies, Her-2/neu expression levels in live breast cancer cell lines can be differentiated by epi-HGM. By injection of tumor cells with CdSe/GEC nanospheres labeling into the dermis tissue of nude mice, the tumor cells can be clearly and continuously imaged with epi-THG microscopy in the subcutaneous tissue over a week.

As eugenics has been concerned more and more in modern days, the health of ovums and embryos play an important role during IVF. In biological concept, there are several ways to score the embryo. Since THG signals reveal the blastomere, the nucleus, and the polar body, and SHG signals show the spindle fibers, we can observe the activation of blastocyst through mitosis which is revealed by SHG. We are able to construct an embryo's morphology through THG signals, while SHG shows that zona pellucida. Although the molecular composition of zona pellucida, the three glycoproteins, ZP1, ZP2, and ZP3, is well-known, the structures of these layers are still unknown. By figuring out the second order nonlinear susceptibility tensor for SHG, we can identify the optical property of these layers. Moreover, after investigated by HGM, the observed embryos were developed normally to ICR mice and this confirmed the least-invasiveness of HGM. With the capability of high penetration, high 3D spatial resolution, and high cell viability, the least invasive HGM provides a unique optical tool for carrying out the job to score the embryos. This research is sponsored by National Health Research Institute of Taiwan (NHRI-EX96-9201EI) and NTU Center for Genomic Medicine.

6. REFERENCE

- ¹ C.-K. Sun, "Higher harmonic generation microscopy," *Adv Biochem Engin/Biotechnol* **95**, 17-56 (2005).
- ² S. W. Chu, I. H. Chen, T. M. Liu, P. C. Chen, and C.-K. Sun, "Multimodal nonlinear spectral microscopy based on a femtosecond Cr:forsterite laser," *Opt. Lett.* **26**, 1909-1911 (2001)
- ³ S. W. Chu, S. Y. Chen, T. H. Tsai, T. M. Liu, C. Y. Lin, H. J. Tsai, and C.-K. Sun, "In vivo developmental biology study using noninvasive multi-harmonic generation microscopy," *Opt. Express* **11**, 3093-3099 (2003)
- ⁴ C.-K. Sun, S. W. Chu, S. Y. Chen, T. H. Tsai, T. M. Liu, C. Y. Lin, and H. J. Tsai, "Higher harmonic generation microscopy for developmental biology," *J. Struct. Bio.* **147**, 19-30 (2004)
- ⁵ S. W. Chu, I. H. Chen, T. M. Liu, C.K. Sun, S.P. Lee, B. L. Lin, P. C. Cheng, M. X. Kuo, D. J. Lin, and H. L. Liu, "Nonlinear bio-photonic crystal effects revealed with multimodal nonlinear microscopy," *J. Microscopy-oxford* **208**, 190-200 Part 3 (2002)
- ⁶ T. Y. F. Tsang, "Optical 3rd-harmonic generation at interfaces," *Phy. Rev. A* **52**, 4116-4125 (1995)
- ⁷ Y. Barad, H. Eisenberg, M. Horowitz, and Y. Silberberg, "Nonlinear scanning laser microscopy by third harmonic generation," *App. Phy. Lett.* **70**, 922-924 (1997)
- ⁸ D.Yelin, and Y. Silberberg, "Laser scanning third-harmonic-generation microscopy in biology," *Opt. Express* **5**, 169-175 (1999)
- ⁹ J. A. Squier, M. Muller, and G. J. Brakenhoff, and K. R. Wilson, "Third harmonic generation microscopy," *Opt. Express* **3**, 315-324 (1998)
- ¹⁰ M. Muller, J. Squier, K. R. Wilson, and G. J. Brakenhoff, "3D microscopy of transparent objects using third-harmonic generation," *J. Microscopy-oxford* **191**, 266-274 (1998)
- ¹¹ A. C. Millard, D. N. Fittinghoff, P. W. Wiseman, M. Muller, G. J. Brakenhoff, J. A. Squier, and K. R. Wilson, "Three dimensional, third harmonic microscopy of living systems," *Biophys. J.* **78**, 800Plat Part 2 (2000)

- ¹² W. Mohler, A. C. Millard, and P. J. Campagnola, "Second harmonic generation imaging of endogenous structural proteins," *Methods* **29**, 97-109 (2003)
- ¹³ P. J. Campagnola, A. C. Millard, M. Terasaki, P. E. Hoppe, C. J. Malone, and W. A. Mohler, "Three-dimensional high-resolution second-harmonic generation imaging of endogenous structural proteins in biological tissues," *Biophys. J.* **82**, 493-508 (2002)
- ¹⁴ K. Konig, P. T. C. So, W. W. Mantulin, E. Gratton, "Cellular response to near-infrared femtosecond laser pulses in two-photon microscopes," *Opt. Lett.* **22**, 135-136 (1997)
- ¹⁵ J. M. Squirell, D. L. Wokosin, J. G. White, and B. D. Bavister, "Long-term two-photon fluorescence imaging of mammalian embryos without compromising viability," *Nat. Biotechnol.* **17**, 763-767 (1999)
- ¹⁶ S. U. Chen, T. H. Lee, Y. R. Lien, Y. Y. Tsai, L. J. Chang, and T. S. Yang, "Microsuction of blastocoelic fluid before vitrification increased survival and pregnancy of mouse expanded blastocysts, but pretreatment with the cytoskeletal stabilizer did not increase blastocyst survival," *Fertility and Sterility* **84**, 1156-1162 (2005).
- ¹⁷ R. D. Schaller, J. C. Johnson, and R. J. Saykally, "Nonlinear chemical imaging microscopy: Near-field third harmonic generation imaging of human red blood cells," *Anal. Chem.* **72**, 5361-5364 (2000).
- ¹⁸ R. Barille, L. Canioni, S. Rivet, L. Sarger, and G. Rivoire, "Nonlinearity measurements of thin films by third harmonic-generation microscopy," *Phys. Rev. E* **66** (2002).
- ¹⁹ J. Thum, L. Caspary, A. Creutzig, and K. Alexander, "New method for the assessment of tissue hemoglobin oxygenation in patients with chronic venous insufficiency," *Microvascular Research* **51**, 317-326 (1996).
- ²⁰ M. Lippitz, M. A. V. Dijk, and M. Orrit, "Third-harmonic generation from single gold nanoparticles," *Nano Lett.* **5**, 799-802 (2005).
- ²¹ C. J. Murphy, "Optical sensing with quantum dots," *Anal. Chem.* **1** 520A-526A (2002).
- ²² D. Debarre, W. Supatto, A. M. Pena, A. Fabre, T. Tordjmann, L. Combettes, M. C. Schanne-Klein, and E. Beaurepaire, "Imaging lipid bodies in cells and tissues using third-harmonic generation microscopy," *Nature Methods* **3**, 47-53 (2006).
- ²³ A. K. Dharmadhikari, N. Kumbhojkar, J. A. Dharmadhikari, S. Mahamuni, and R. C. Aiyer. "Studies on third-harmonic generation in chemically grown ZnS quantum dots," *J. Phys.: Condens. Matter* **11**, 1363-1368 (1999).
- ²⁴ S. V. Popruzhenko, D. F. Zaretsky, and W. Becker, "Third harmonic generation by small metal clusters in a dielectric medium," *J. Phys.* **B 39**, 4933-4943 (2006).
- ²⁵ S. Cooke, J. P. P. Tyler, G. L. Driscoll, "Meiotic spindle location and identification and its effect on embryonic cleavage plane and early development," *Human Reproduction* **18**, 2397-2405 (2003).
- ²⁶ S. Y. Chen, C. S. Hsieh, S. W. Chu, C. Y. Ko, Y. C. Chen, H. J. Tsai, C. H. Hu, C. K. Sun, "Noninvasive harmonics optical microscopy for long-term observation of embryonic nervous system development *in vivo*," *J. Biom. Opt.* **11**, 054022-054029 (2006).
- ²⁷ T. R. Shen, *The Principles of Nonlinear Optics*, John Wiley & Sons, Hoboken, NJ, USA, 2002.